Geophys. J. Int. (2000) **143,** 507–520

Calculating splitting parameters for plume-type anisotropic structures of the upper mantle

Georg Rümpker[1] and Paul G. Silver[2]

[1] *GeoForschungsZentrum Potsdam, Telegrafenberg,* 14473 *Potsdam, Germany. E-mail: rumpker@gfz-potsdam.de*
[2] *Department of Terrestrial Magnetism, Carnegie Institution of Washington,* 5241 *Broad Branch Road, NW, Washington,* DC 20015, *USA*

Accepted 2000 April 3. Received 2000 April 3; in original form 1999 November 3

SUMMARY

We apply a forward-propagator method to calculate shear wave splitting parameters for general (3-D) weakly anisotropic upper mantle structures. The approach is valid under the assumption that the ray paths of the two quasi-shear (qS) waves can be approximated by a common reference ray within an isotropic background medium. Along the reference ray the incremental splitting is expressed in terms of qS polarizations and slownesses in the direction of propagation. Using a ray theory ansatz, we show that the resulting shear wave seismogram is equivalent to the coupling ray theory of Coates & Chapman (1990) under the assumption of smoothly varying anisotropy. Here, we use the forward-propagator method to calculate apparent shear wave splitting parameters that can be compared directly with observations of teleseismic shear wave splitting. A comparison with finite difference calculations is used to assess the validity of the method. As an application we consider shear wave splitting due to a plume-type anisotropic upper mantle structure. The anisotropy is assumed to result from the preferred alignment of orthorhombic olivine. We show examples of waveforms and splitting parameters as functions of backazimuth and angle of incidence. Anisotropic effects for *SKS* are weak at stations near the central upwelling due to the combined effects of initial polarization and olivine *a*-axis orientation. Here, the splitting parameters are irregular and fast-axis directions may vary by up to 70° depending on the vertical incidence angle. At larger distances splitting parameters slowly converge towards values expected for homogeneous media. The results suggest that direct evidence for mantle plumes from shear wave splitting is more likely to come from (OBS) stations at some distance away from the central upwelling. At shallower incidence, the apparent splitting parameters for *S* exhibit a 90° periodicity as functions of the initial polarization of the incident shear wave, provided that the ray path is kept fixed. Our results show that this is a general characteristic of shear wave splitting in inhomogeneous anisotropic media. The effect can be used to identify complex anisotropic regions within the Earth's mantle.

Key words: 3-D media, mantle plume, shear wave splitting, weak anisotropy.

1 INTRODUCTION

The analysis of shear wave splitting observations is usually performed in terms of the polarization direction of the fast shear wave (ϕ) and the delay time between the fast and slow shear wave (δt) (e.g. Silver & Chan 1991; Vinnik & Kind 1993). For a single homogeneous anisotropic region, the relationship between the observed splitting parameters (ϕ, δt) and the anisotropic properties of the medium is relatively straightforward: given the elastic constants and the orientation (slowness) of the incident wave front, shear wave phase velocities and polarizations correspond to eigenvalues and eigenvectors of the anisotropic Christoffel equation (e.g. Musgrave 1970). The delay times can be calculated from the different qS phase velocities if the extent of the anisotropic region is known. It is usually assumed that seismic anisotropy of the upper mantle is caused mainly by the lattice-preferred orientation (LPO) of orthorhombic olivine. Direct evidence for this comes from petrofabric analyses of upper mantle xenoliths and peridotites (e.g. Nicolas & Christensen 1987; Mainprice & Silver 1993; Peselnik & Nicolas 1978). The crystal alignment is a response to the finite strain associated with differential mantle flow, where the olivine *a*-axis tends to be oriented parallel to the principal extension direction (McKenzie 1979; Ribe & Yu 1991; Wenk *et al.* 1991; Silver *et al.* 1999). A number of numerical studies have considered crystallographic texture evolution in response to deformation and flow processes

in the upper mantle. The development of seismic anisotropy has been investigated for passive and buoyant flows along a spreading ridge (Blackmann *et al.* 1996), and flows induced by plate motion (Tommasi *et al.* 1996; Tommasi 1998) and mantle convection (Chastel *et al.* 1993; Dawson & Wenk 1997). Alternatively, the orientations of the crystallographic axes may be constrained directly from the finite strain associated with the flow field. This approach was used in the modelling of mantle flows and anisotropy related to continental keels (Fouch *et al.* 2000) and back-arc spreading (Hall *et al.* 2000). Upper mantle regions of variable anisotropy are a common feature in these numerical simulations. The polarization of shear waves propagating in inhomogeneous anisotropic media may be highly variable due to ray path curvature and changes in crystal orientation. Consequently, the relationship between observed fast polarization directions and the olivine crystallographic axes is obscured.

For vertical shear wave propagation in layered anisotropic media, the observations can still be characterized by two *apparent* splitting parameters, ϕ_a and δt_a (Silver & Savage 1994; Rümpker & Silver 1998), provided that the dominant period of the incident wave is large compared to the accumulated delay time. Rümpker & Silver (1998) found systematic relationships between ϕ_a and the horizontal *a*-axis orientations in a smoothly varying medium. An important characteristic of layered anisotropy is the 90° periodicity of the apparent splitting parameters as functions of backazimuth. In this paper we show that the concept of apparent splitting parameters also applies to general anisotropic media provided that the anisotropy is relatively weak, such that the *qS* ray paths can be approximated by a single (reference) ray. Analytical expressions of apparent splitting parameters have been derived for two-layer and multilayered anisotropic media (Silver & Savage 1994; Rümpker & Silver 1998). Inversions of splitting observations based on these models can be performed to resolve depth-dependent structures beneath a station. However, this requires the determination of splitting parameters for a wide range of initial polarizations (or backazimuths in the case of core phases such as *SKS*). The results of the inversion can be ambiguous and depend on the assumed 'starting model' (Rümpker *et al.* 1999). Forward calculations of splitting parameters have the advantage that the results can be compared directly with splitting measurements on observed seismograms. This avoids the additional step of performing splitting measurements on synthetic waveforms. In this paper we calculate apparent splitting parameters by applying a forward-propagator formalism (Rümpker & Silver 1998) to the rays in the 3-D medium. The complete forward-propagator seismogram can be expressed in terms of a single matrix operator applied to the incident waveform. The general form of the operator remains the same for inhomogeneous and for one-layer anisotropic media. The apparent splitting parameters ϕ_a and δt_a can be defined by comparison between the two operators.

In earlier studies, *qS*-wave seismograms for weakly anisotropic media were derived on the basis of a representation theorem (Coates & Chapman 1990) and by a ray theoretical approach (e.g. Sharafutdinov 1994; Pšenčík 1998; Zillmer *et al.* 1998). In both cases, perturbation theory was used to derive the seismograms, and the final expressions have been shown to be identical (Pšenčík 1998; Zillmer *et al.* 1998). Under the assumption of a common ray path, the methods describe the coupling between the two shear waves, which is caused by changes in polarization along the ray. Here we focus on the derivation of apparent splitting parameters by using a straightforward generalization of the splitting operator formalism. It turns out that the resulting seismogram is again equivalent to the coupling theory of Coates & Chapman (1990). The applicability to shear wave splitting calculations for typical upper mantle anisotropic structures is assessed by comparison with finite difference calculations using a parabolic approximation method. As an application, we consider shear wave splitting parameters for a simplified anisotropic plume structure.

2 THEORY

In this section, we describe a numerical formalism for the calculation of the shear wave seismogram in general weakly anisotropic media. Our goal is the application of this formulation to the calculation of splitting parameters, which will allow direct comparison with shear wave splitting measurements. We start with the usual ansatz for the frequency-domain shear wave displacement **u** (e.g. Silver & Chan 1991):

$$\mathbf{u} = u(\omega)\mathbf{\Gamma}\cdot\hat{\mathbf{p}}\,, \tag{1}$$

where $u(\omega)$ denotes the waveform of the incident shear wave, $\hat{\mathbf{p}}$ is the corresponding initial polarization and $\mathbf{\Gamma}$ is the splitting operator, which usually accounts for the effect of a single anisotropic layer on the vertically incident wave. The generalization of (1) to multiple anisotropic layers in terms of a forward propagator method is described in Rümpker & Silver (1998). To derive a similar formulation for curved ray paths in 3-D media, we use the fact that, in weakly anisotropic media, the ray paths of the two *qS* waves are similar and may be approximated by the shear wave path in an isotropic reference medium (Coates & Chapman 1990). We argue that anisotropic effects may be accounted for by successive applications of splitting operators along the reference ray. This approximation breaks down in strongly anisotropic media where the (multiple) *qS* ray paths may rapidly diverge. Note that this problem does not arise for vertical one-way propagation in layered media due to the unique ray path.

In view of the numerical calculations, we express the arc length along the reference ray, x, in discretized form: $x_k = k\Delta x$, where Δx denotes an incremental segment along the ray. The corresponding incremental splitting operator at x_k is given by

$$\mathbf{\Gamma}_k = \mathrm{e}^{-i\omega\delta t_k/2}\,\hat{\mathbf{f}}_k\hat{\mathbf{f}}_k + \mathrm{e}^{+i\omega\delta t_k/2}\,\hat{\mathbf{s}}_k\hat{\mathbf{s}}_k\,, \tag{2}$$

where

$$\delta t_k = [p_s(x_k) - p_f(x_k)]\,\Delta x\,, \tag{3}$$

is the incremental delay time. The unit vectors $\hat{\mathbf{f}}_k$ and $\hat{\mathbf{s}}_k$ are the polarizations of the fast and slow shear waves at x_k, and p_s and p_f are the corresponding slownesses in the direction of propagation. Both the polarizations and the slownesses in the direction of the reference ray can be obtained from the eikonal equation for the anisotropic medium (Musgrave 1970) using standard numerical methods. Analytical expressions that are valid in the limit of weak anisotropy have been derived by Jech & Pšenčík (1989) using degenerate perturbation theory (Landau & Lifshitz 1977). At this point, we are not concerned with the details of these calculations. We note, however, that the polarizations $\hat{\mathbf{f}}_k$ and $\hat{\mathbf{s}}_k$ are orthogonal in the limit of weak anisotropy (Coates & Chapman 1990).

A factor $\exp(i\omega p_0 \Delta x)$, where $p_0 = (p_s + p_f)/2$, is usually omitted from the seismogram. Thus, the displacement is obtained in the reduced time domain $t' = t - p_0 \Delta x$. We continue by writing the displacement at x_k:

$$\mathbf{u}_k = u_k^{(f)} \hat{\mathbf{f}}_k + u_k^{(s)} \hat{\mathbf{s}}_k \,, \tag{4}$$

where the orthogonality of $\hat{\mathbf{f}}_k$ and $\hat{\mathbf{s}}_k$ is assumed, and $u_k^{(f)}$, and $u_k^{(s)}$ are the corresponding displacement components. By generalization of (1), the effect of the incremental splitting operator on the displacement may now be expressed in the form

$$\mathbf{u}_k = \mathbf{\Gamma}_k \mathbf{u}_{k-1} \,. \tag{5}$$

In (5) we assume that the operator $\mathbf{\Gamma}_k$ is given in matrix form,

$$\begin{pmatrix} u_k^{(f)} \\ u_k^{(s)} \end{pmatrix} = \begin{pmatrix} \cos\Delta\xi_k \, \mathrm{e}^{-i\omega\delta t_k/2} & \sin\Delta\xi_k \, \mathrm{e}^{-i\omega\delta t_k/2} \\ -\sin\Delta\xi_k \, \mathrm{e}^{+i\omega\delta t_k/2} & \cos\Delta\xi_k \, \mathrm{e}^{+i\omega\delta t_k/2} \end{pmatrix} \begin{pmatrix} u_{k-1}^{(f)} \\ u_{k-1}^{(s)} \end{pmatrix}, \tag{6}$$

where $\Delta\xi_k$ is defined by

$$\hat{\mathbf{f}}_k \cdot \hat{\mathbf{f}}_{k-1} = \cos\Delta\xi_k \tag{7}$$

and denotes an angular change of polarization across Δx.

For given initial displacement components, $u_0^{(f)}$ and $u_0^{(s)}$, eq. (6) may be used to calculate iteratively the displacement along the reference ray. We assume that polarizations and slownesses along the ray have been obtained from the eikonal equation for the anisotropic medium. The polarizations may change discontinuously along the reference ray due to changes in medium properties or related to slowness surface singularities (e.g. Crampin 1981). No assumptions have been made regarding the size of $\Delta\xi_k$. However, in view of numerical calculations in inhomogeneous media, we require that Δx is chosen sufficiently small such that $\delta t_k(\Delta x)/\Sigma\,\delta t_k \ll 1$, where $\Sigma\,\delta t_k$ is the total accumulated delay time along the complete ray path within the anisotropic region.

Under the assumption of a smoothly varying weakly anisotropic medium, it can be shown that our formulation (6) is equivalent to the coupling ray theory of Coates & Chapman (1990) (see Appendix A), which was derived on the basis of a representation theorem for the displacement. This also implies equivalence with the so-called quasi-isotropic approximation (see e.g. Zillmer *et al.* 1998 for details).

In eq. (6) the displacement is expressed with respect to $\hat{\mathbf{f}}$–$\hat{\mathbf{s}}$ coordinates, which are given by the rotating fast and slow polarizations along the reference ray. For the application of eq. (6) to the calculation of apparent splitting parameters, it is convenient to express the displacement with respect to the ray-centred coordinate system of the reference ray with mutually orthogonal unit vectors ($\hat{\mathbf{p}}$, $\hat{\mathbf{p}}_\perp$, $\hat{\mathbf{x}}$). In ray-centred coordinates the polarizations $\hat{\mathbf{p}}$, $\hat{\mathbf{p}}_\perp$ do not change along the ray (Červený 1987). They may rotate, however, with respect to a global (Cartesian) coordinate system. Also, for vertical propagation or within a homogeneous reference medium, the Cartesian components of $\hat{\mathbf{p}}$ remain constant. For near-vertical incidence, the two orthogonal vectors $\hat{\mathbf{p}}$ and $\hat{\mathbf{p}}_\perp$ may be denoted as the initial shear wave polarization and its orthogonal, or simply the radial and transverse directions in the case of core phases (e.g. Rümpker & Silver 1998).

Thus,

$$\begin{pmatrix} \hat{\mathbf{f}}_k \\ \hat{\mathbf{s}}_k \end{pmatrix} = \begin{pmatrix} \cos\phi_k & \sin\phi_k \\ -\sin\phi_k & \cos\phi_k \end{pmatrix} \begin{pmatrix} \hat{\mathbf{p}} \\ \hat{\mathbf{p}}_\perp \end{pmatrix} \equiv \mathbf{T}_k \begin{pmatrix} \hat{\mathbf{p}} \\ \hat{\mathbf{p}}_\perp \end{pmatrix}, \tag{8}$$

where ϕ_k denotes the angular distance between $\hat{\mathbf{f}}_k$ and $\hat{\mathbf{p}}$ as defined by

$$\hat{\mathbf{f}}_k \cdot \hat{\mathbf{p}} = \cos\phi_k \,. \tag{9}$$

Also note that $\Delta\xi_k = \phi_k - \phi_{k-1}$. In view of (5), the displacement along the reference ray may then be calculated from

$$\mathbf{u}_k^{(p)} = \mathbf{T}_k^{-1} \mathbf{\Gamma}_k \mathbf{T}_{k-1} \mathbf{u}_{k-1}^{(p)} = \mathbf{\Gamma}_k^{(p)} \mathbf{u}_{k-1}^{(p)} \,, \tag{10}$$

where $\mathbf{T}_k$ denotes the transformation matrix defined by (8) and the superscript refers to the ray-centred coordinate system. In view of (6) and (10), the propagator $\mathbf{\Gamma}_k^{(p)}$ can be given in the form

$$\mathbf{\Gamma}_k^{(p)} = \begin{pmatrix} a_k & b_k \\ -\bar{b}_k & \bar{a}_k \end{pmatrix}. \tag{11}$$

with

$$a_k = \cos\theta_k - i\sin\theta_k\cos\alpha_k \,, \qquad b_k = -i\sin\theta_k\sin\alpha_k \,, \tag{12}$$

and $\theta_k = \omega\delta t_k/2$, $\alpha_k = 2\phi_k$ (the bar denotes the complex conjugate).

The propagator (11) is formally equivalent to the forward propagator derived by Rümpker & Silver (1998) for vertical propagation in layered anisotropic media. Consequently, the expressions for apparent splitting parameters derived in that paper may be applied directly to our present formulation. Apparent splitting parameters can be calculated under the assumption that anisotropic effects on the incident waveform are caused by a single anisotropic layer (e.g. Silver & Savage 1994). In this case, the splitting may be characterized by only two parameters: the apparent polarization of the fast shear wave (ϕ_a) and the apparent delay time between the fast and slow shear waves (δt_a). The parameters are meaningful only at relatively long periods when multiple arrivals are indistinguishable. The expression (10) implies that this concept also applies to general weakly anisotropic media and that, at long periods, anisotropic effects along the reference ray may be characterized by only two parameters. To derive the apparent splitting parameters for a ray segment ranging from x_0 to x_N, where x_0 corresponds to the initial point of anisotropy, we formally equate

$$\mathbf{u}_N^{(p)} = \mathbf{\Gamma}_{N,1}^{(p)} \mathbf{u}_0^{(p)} \equiv K \mathbf{\Gamma}_a \mathbf{u}_0^{(p)} \,, \tag{13}$$

where $\mathbf{\Gamma}_{N,1}^{(p)} = \mathbf{\Gamma}_N^{(p)} \ldots \mathbf{\Gamma}_1^{(p)}$ is the complete forward propagator and $\mathbf{\Gamma}_a$ is the apparent splitting operator. The complex scalar K accounts for an arbitrary time shift (Silver & Savage 1994). Explicit expressions for ϕ_a and δt_a have been derived by Rümpker & Silver (1998) and are also given in Appendix B. The apparent splitting parameters exhibit a 90° periodicity with respect to the initial polarization $\hat{\mathbf{p}}$ of the incident wave. This periodicity was first noted for vertical-propagation media with two (Silver & Savage 1994) and multiple (Rümpker & Silver 1998) anisotropic layers. Here, it applies to a fixed (but arbitrary) ray path in a general weakly anisotropic medium. Note that the forward propagator is invariant to polarization changes $\phi_k \pm \pi$ (see eq. 12). Thus, eq. (13) can be applied without difficulty to the numerical calculation of waveforms and splitting parameters near slowness surface singularities.

3 NUMERICAL EXAMPLES

3.1 Plume model

As an application of our method we consider the effects of 3-D anisotropic variations due to a simplified mantle plume structure. The model is defined within the top 400 km of the upper mantle with anisotropy due to the lattice preferred orientation (LPO) of olivine crystals. Detailed modelling of olivine texture development for plume-type mantle upwellings is not yet available. Therefore, we have chosen a phenomenological approach and have designed a plume model in view of mineral texture calculations for mid-ocean-ridge upwellings by Blackman *et al.* (1996) (see also Blackman & Kendall 1997). The authors discriminate between a passive, plate-driven upwelling and a buoyancy-enhanced upwelling. The latter exhibits pronounced vertical alignment of olivine *a*-axes near the ridge axis. Both models are characterized by more or less horizontal *a*-axis orientations at some distance away from the axis. Here, similar to the plume modelling of Martin & Thomson (1997), we have adopted the findings of Blackman *et al.* (1996). The resulting 3-D axisymmetric model is depicted in Fig. 1. Solid bars denote the orientation of the olivine *a*-axis, the lengths of which correspond to the strength of the anisotropy. The anisotropy decreases gradually with increasing distance from the centre, more rapidly at greater depth. At the centre the olivine *a*-axis is aligned vertically; at larger distances the *a*-axis gradually aligns with the horizontal. The width of the transition between central and peripheral regions increases with depth. Olivine elastic constants have been taken from Kumazawa & Anderson (1969). We assume a peridotite mantle consisting of 70 per cent olivine, 60 per cent of which exhibits a preferred alignment. The complete elastic tensor is thus given by an anisotropic portion of orthorhombic symmetry (due to aligned olivine) and a remaining isotropic portion in the form

$$c_{ijkl} = 0.7 \times 0.6\, c^{(a)}_{ijkl} + (1 - 0.7 \times 0.6)\, c^{(i)}_{ijkl}\,. \qquad (14)$$

The isotropic background medium is assumed homogeneous with isotropic velocities $v_P = 9.2$ km s^{-1} and $v_S = 4.9$ km s^{-1}, which is close to the average velocity in the upper mantle at 400 km depth. Thus, we are ignoring the anisotropic contribution of the lithosphere and also the possible interaction between the upwelling and lithospheric plate movement (Ribe & Christensen 1994; Savage & Sheehan 1999). However, within our model this is justified due to the relatively large contribution from anisotropy in the deeper parts of the upper mantle. We follow the procedure of Kendall & Thomson (1993a) by choosing the Voigt–Hill average velocities of the anisotropic portion equal to the *P* and *S* velocities of the isotropic portion. The resulting elastic medium exhibits an accumulated delay time of 1 s over a distance of 150 km in directions perpendicular to the *a*-axis. This corresponds to about 3 per cent of anisotropy, which is compatible with measurements of velocity variations on mantle xenoliths as described by e.g. Mainprice & Silver (1993). The incremental splitting operator is calculated along reference rays within an isotropic background medium with elastic constants given by the isotropic elastic tensor in (14).

3.2 Testing the method

When applying the forward propagator to 3-D media we assume that the ray paths of the two *qS* waves are sufficiently close such that the separation between the rays is small and their paths can be approximated by a single reference ray. Media for which this approximation holds are denoted as weakly anisotropic. It remains to be shown that this assumption is justified in our modelling of relatively long-period waveforms such as *SKS*. Additionally, inhomogeneities of velocity and anisotropy affect the wavefield within a certain volume surrounding the reference ray. The forward propagator only accounts for variations of anisotropy in the direction of the reference ray path. We test the applicability of our method to the modelling of upper mantle *SKS* propagation by comparison with a one-way finite difference method, which is based

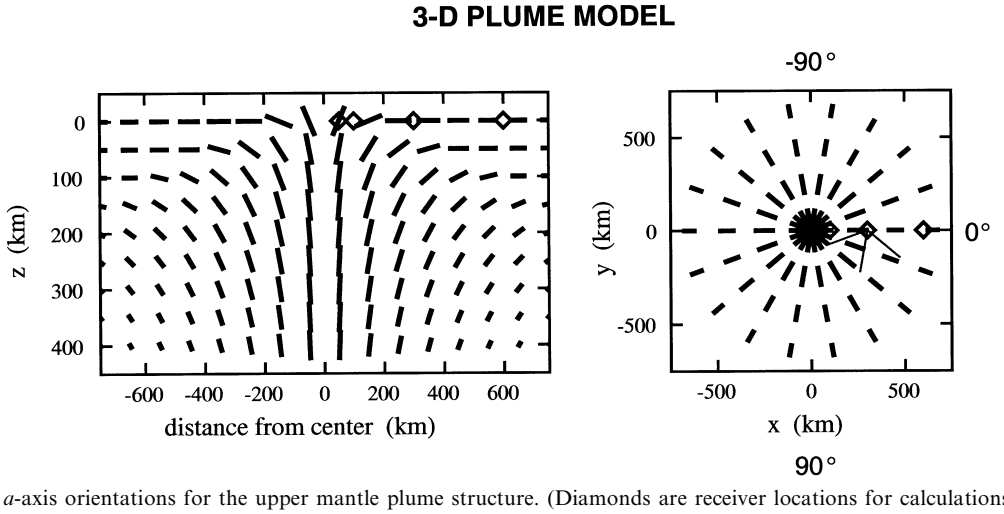

Figure 1. Olivine *a*-axis orientations for the upper mantle plume structure. (Diamonds are receiver locations for calculations given in Fig. 4.) (Left) A vertical section through the centre of the 3-D axisymmetric model. The *a*-axes (solid bars) are vertical in the centre and align horizontally at larger distances. The lengths of the bars correspond to the strength of the anisotropy. The *b*-axis lies within the plane of the paper perpendicular to the *a*-axis. The *c*-axis points out of this plane. (Right) Bird's-eye view of the plume structure. At the surface, the *a*-axes point in the radial direction; they are vertical at the centre $x = y = 0$. In our model, fast polarizations and backazimuths of 0° and 180° correspond to directions parallel to the *x*-axis, whereas ±90° corresponds to directions parallel to the *y*-axis. The solid lines denote (horizontal) ray path projections of examples given in Fig. 6.

on a parabolic approximation to the anisotropic wave equation (Rümpker 1996). This method accounts for forward scattering and wavefield smoothing effects in variable media at relatively low frequencies. Wavefield calculations based on finite difference techniques are much more time-consuming, even in 2-D media. Also, the direct calculation of splitting parameters is not possible, as the displacement field cannot be expressed in terms of a simple splitting operator. For the comparison, we obtain splitting parameters by measurements on synthetic finite difference waveforms using the usual grid-search method (e.g. Silver & Chan 1991). For simplicity, we consider a 2-D section of our plume model (the vertical plane at $y=0$ km). A plane horizontal shear wave front enters the model at the base and travels vertically upwards through the anisotropic upper mantle over a distance of 400 km. Waveforms are calculated for two cases: (i) the plane of propagation coincides with the *a–b* symmetry plane of olivine—this corresponds to the situation depicted in Fig. 1; (ii) the plane of propagation coincides with the *a–c* symmetry plane of olivine. This case is not directly linked to the flow field of our plume model. However, it simply serves as an additional example for the comparison between the two methods. In both cases the *a*-axis is vertical within the central upwelling. For larger distances the *a*-axis gradually aligns with the horizontal. There, either (i) the *b*-axis or (ii) the *c*-axis is oriented vertically, parallel to the direction of propagation.

To simplify the interpretation of the results we note that for shear waves propagating parallel to the *a*-axis, the fast polarization is oriented parallel to the *b*-axis and the splitting is relatively weak (<1 per cent anisotropy). On the other hand, for propagation along the *b*- or *c*-axis, the fast polarization is oriented parallel to the *a*-axis, and the splitting is more pronounced (≈ 3 per cent anisotropy). Furthermore, within the *a–c* symmetry plane of olivine, there are four directions (about 15° away from the *a*-axis) for which the *qS*-wave speeds coincide, and where the medium is locally isotropic. Polarizations along the reference rays are obtained from the Christoffel equation, which is solved by numerical means. The polarization directions are undetermined by $\pm 180°$. However, this has no effect on the evaluation of the forward propagator (11) or the apparent fast polarization (B4). The delay time is calculated from the slowness differences $(p_s - p_f)$ in the direction of propagation at a given x_k. To maximize the effects of the anisotropy on the incident wave we choose an initial polarization of 45° between the *x*- and *y*-axes (Fig. 1). The initial waveform is given by the derivative of a Gaussian with a dominant period of 8 s.

In Fig. 2, we compare apparent splitting parameters for the two methods. The results for the forward propagator have been obtained by direct calculation (using eqs B3 and B4) and, in addition, by splitting measurements on synthetic waveforms (10). The good agreement between calculations and measurements indicates that calculated forward-propagator results may be compared directly with measurements on finite difference waveforms. Thus, any disagreement between calculated and measured splitting parameters is most likely to be due to inherent differences between the two methods. In Fig. 2(a), the forward propagator predicts a fast-axis direction $\phi_a = 0°$ for the complete distance range, which is expected for propagation within the *a–b* symmetry plane. The apparent delay time exhibits variations between 1 and 1.6 s, with a minimum at the centre of the model, where the *a*-axis is vertical, and the splitting in the direction of propagation is relatively small. Close to the centre, the apparent fast axes for the finite difference calculations are slightly more variable, while the delay times agree well. This is probably due to stronger lateral variations close to distances of ± 100 km (see Fig. 1). However, the absolute differences are smaller than 7°, which is negligible in view of measurements on real data. In Fig. 2(b), the forward propagator predicts fast-axis directions of $-90°$ within the central region and of 0° for larger distances. This is expected for propagation within the *a–c* plane as the out-of-plane *b*-axis corresponds to the fast direction for propagation parallel to the *a*-axis (Verma 1960). The apparent delay time varies between 0 and 1.7 s and exhibits minima at ± 100 km, which is related to directions of local isotropy described earlier. Here, the determination of splitting parameters fails due to the negligibly small transverse component. The minima coincide with abruptly changing fast-axis directions, where differences between the two methods are most pronounced. Apparent fast axes differ by up to 23°; the differences between the delay times remain relatively small. Away from this, the agreement is good.

In view of these results we conclude that the forward propagator can be applied effectively to the prediction of splitting parameters in variable anisotropic regions. However, a careful interpretation of the results is required whenever the energy on the transverse component is relatively small, which results in larger uncertainties for the apparent splitting parameters.

3.3 Splitting parameters

Returning to the 3-D plume model, we calculate apparent splitting parameters for receiver positions at various distances from the plume centre (see Fig. 1). We consider *SKS* rays entering the base of the plume region at incidence angles θ of 5° and 25° (with respect to the vertical, Fig. 3). These values approximately correspond to upper and lower bounds of *SKS* incidence angles. As before, the reference rays propagate within a homogeneous isotropic background medium. Ray curvature is neglected as θ varies by less than 5° between depths of 300 and 100 km (based on the IASPEI91 model of Kennett & Engdahl 1991), which is negligible compared to effects due to variations of anisotropy in our model. First, we analyse the strength of anisotropic effects on the waveforms as a function of backazimuth (see Fig. 3) and distance from the plume centre. We consider a range of receiver positions along a profile $y=0$, $x>0$. At each receiver, seismograms are calculated for a range of backazimuths between 0° and 180°. For *SKS* the backazimuth is equal to the initial polarization. The strength of anisotropic effects is calculated from the quotient of energy on the transverse and radial displacement components, $q = E_t/E_r$. Obviously, $q=0$ in the isotropic case. However, we also have $q=0$ whenever the initial polarization is oriented parallel to the fast or slow polarization along the complete ray path. Anisotropic effects are most pronounced in regions where $q \approx 1$.

Fig. 4 shows contours of q for the two incidence angles of 5° and 25°. In both cases, values of q are largest at distances between about 150 and 450 km. In our model, anisotropy decreases continuously with distance. However, for rays arriving at a receiver directly above the centre, the fast polarization direction is always parallel to the radial direction (for any backazimuth). In addition, the anisotropy is relatively weak for

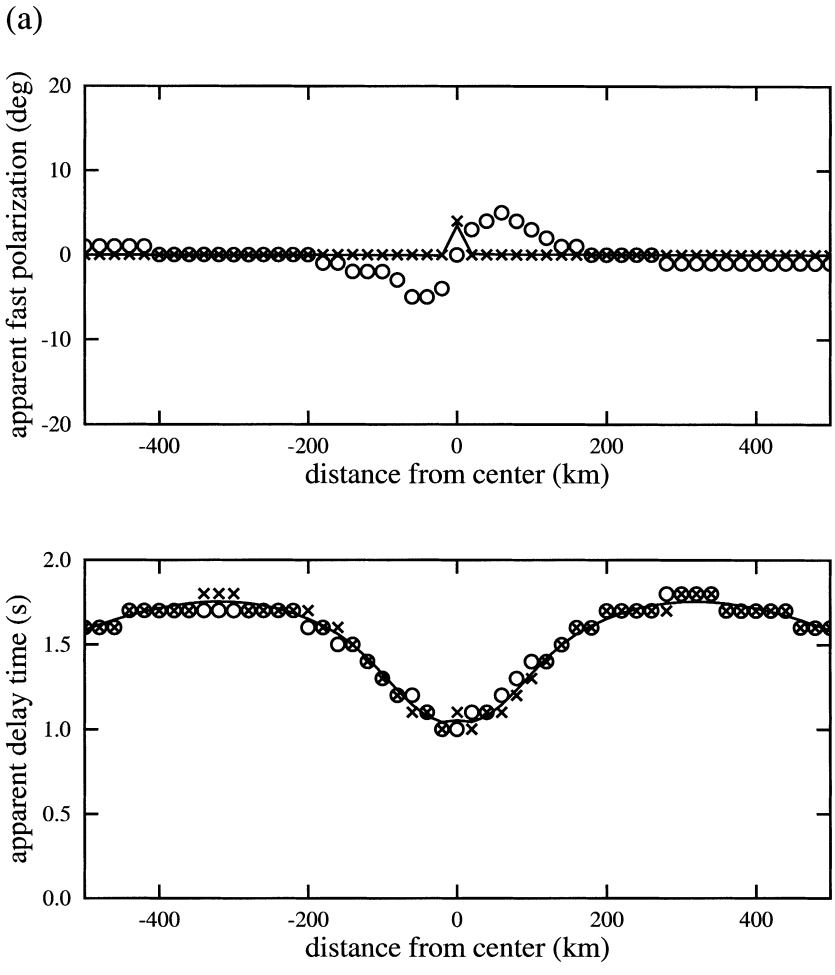

Figure 2. Apparent splitting parameters along a profile ($y=0$) through the centre of the plume. Calculated splitting parameters (solid lines) are compared with measurements on forward-propagator waveforms (crosses) and on finite difference waveforms (circles). The results are given for vertical incidence with an initial polarization of 45° between x and y. The dominant period is 8 s. (a) The orientations of the olivine crystallographic axes are the same as in the plume model of Fig. 1. (b) The b-axis and the c-axis are exchanged.

propagation parallel to the a-axis. Both effects cause small values of q near the centre ($x<100$ km). At relatively steep incidence ($\theta=5°$), values of q remain small for backazimuths of 0°, 90° and 180°. These values correspond to the dominant fast and slow polarization directions in the medium. This effect is somewhat smeared out for more oblique incidence ($\theta=25°$). As a result, values of q are largest near a backazimuth of 90°.

Now we consider four receiver positions (Fig. 1) along the profile ($y=0$) in greater detail. At each receiver, apparent splitting parameters are calculated for a complete range of backazimuths from 0° and 358° at increments of 2° (Fig. 5). The splitting parameters as functions of backazimuth exhibit symmetries due to the axial symmetry of the plume model: the apparent delay times are symmetric with respect to backazimuths of 0° (or 360°) and 180°. The apparent fast polarization directions exhibit a similar symmetry when further reflected with respect to $\phi_a=0°$. However, as expected for 3-D variations of anisotropy and oblique incidence, the apparent splitting parameters are non-periodic with respect to backazimuth. The backazimuthal variations are less pronounced at near-vertical incidence ($\theta=5°$). Note that at strictly vertical incidence the splitting parameters are independent of backazimuth or initial polarization in our model. This is because the fast polarization direction, which remains within the a–b symmetry plane (parallel to the x-axis), is independent of depth. (For vertical propagation the fast polarization is parallel to the azimuth of a given receiver position. Along the x-axis this corresponds to $\phi_a=0°$.)

In our examples, at $\theta=5°$, the apparent fast polarization varies between $\phi_a=\pm25°$ and the apparent delay time between $\delta t_a=0.5$ s and $\delta t_a=2.1$ s. Closer to the centre, ϕ_a is more variable, reflecting the more rapid variations of anisotropy within the medium. For larger distances the apparent splitting parameters converge towards the values expected for vertical incidence ($\phi_a=0°$, $\delta t_a=1.3$ s). Rapid variations of δt_a occur near backazimuths of 90° and 270°. Anisotropic effects, however, are relatively small for these directions as the initial polarization is more or less parallel to the slow polarization direction within the medium.

For $\theta=25°$, the apparent splitting parameters are more variable with both changes in backazimuth and increasing distance from the centre. At 50 km the apparent fast polarizations cover the entire range between $\pm90°$. However, pronounced splitting only occurs for backazimuths between 45°

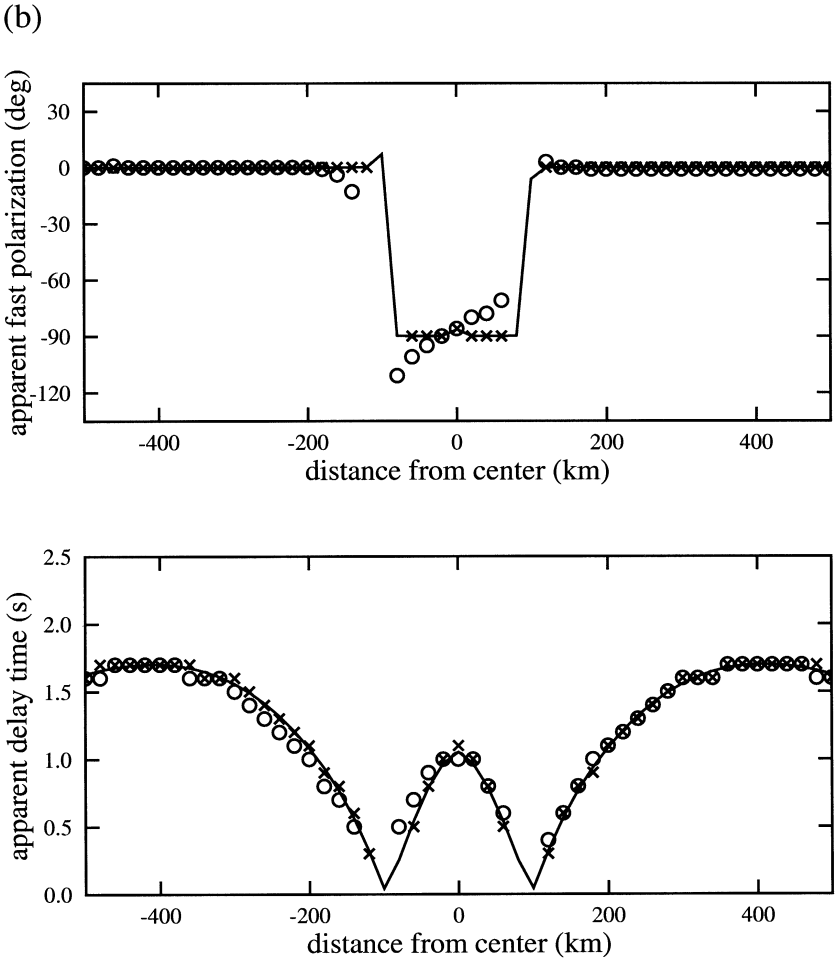

Figure 2. (*Continued.*)

and 135° (and similarly between 225° and 315°), where ϕ_a varies linearly from 45° over $\pm 90°$ to $-45°$. The corresponding delay times are close to 1 s. Note that the *a*-axis at this distance is near-vertical, such that for backazimuths near 90° much of the propagation occurs within the *a–c* symmetry plane. Thus, as θ is relatively large, the fast polarization is close to $\phi_a = \pm 90°$ for much of the ray path. At larger distances (300 km) the *a*-axis is more horizontal and fast polarizations along the rays are closer

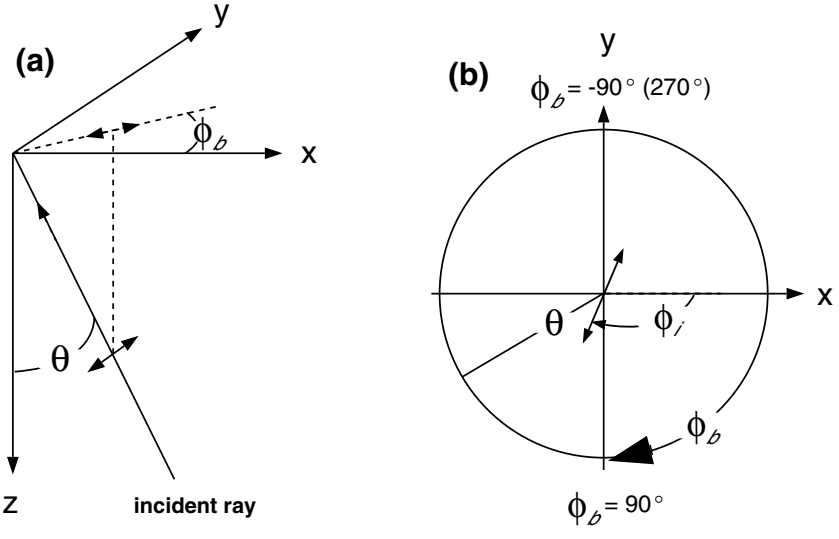

Figure 3. Parameters of the incident ray with respect to the coordinate system used in Fig. 1. (a) The backazimuth ϕ_b and the vertical angle of incidence θ. (b) The angle ϕ_i is given by the projection of the incident shear wave polarization into the horizontal plane. For core phases such as *SKS* the angle ϕ_i is equal to the backazimuth ϕ_b.

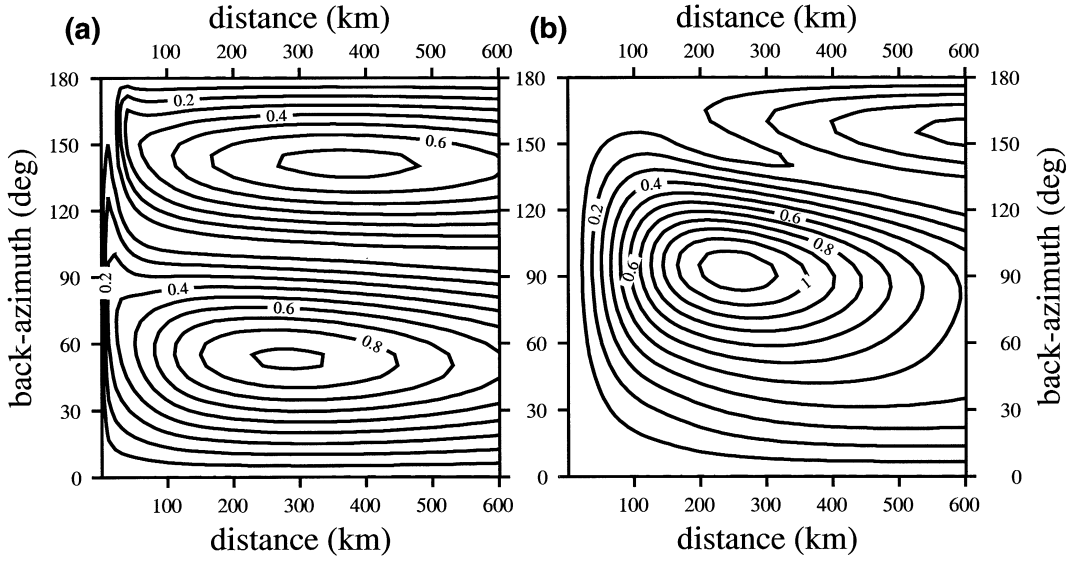

Figure 4. Contours of the relative energy on the transverse displacement component, $q = E_t/E_r$, as functions of backazimuth and distance from the plume centre. The receivers are located along $y = 0$. The vertical angle of incidence is (a) $\theta = 5^\circ$ and (b) $\theta = 25^\circ$.

to the *a–b* symmetry plane. Thus, ϕ_a is less variable with values between $\pm 50^\circ$. The delay time exhibits variations between 0.5 and 2.5 s; this is most pronounced near backazimuths of 150° and 210°, where delay times change by about 2 s. At 600 km, the splitting parameters are most variable at backazimuths of about 120° and 240°. Here δt_a exhibits extreme values of 0.5 and 3 s, and ϕ_a changes by about 40°. However, q values are relatively small in this case.

3.4 Effects of backazimuth and initial polarization

In an isotropic radially symmetric earth the initial polarization of *SKS* is equal to the backazimuth of the source location (see Fig. 3). The phase enters the upper mantle region at relatively steep angles $\theta < 25^\circ$. At shallower incidence (in the case of *S*), the initial polarization can usually be determined from a moment tensor solution or, at sufficiently long periods, directly from a particle motion analysis at the receiver. In this section we study the effects of the initial polarization of *S* in more detail. In Fig. 6, we show 'true' fast polarizations along reference ray paths for shear waves that enter the upper mantle model at a (vertical) incidence angle of 30°. To account for the effects of azimuthal variations we chose backazimuths of $\phi_b = 40^\circ$, 100°, 160° at a fixed receiver position of 300 km. (We found that variations of fast polarizations along ray paths are somewhat more pronounced at intermediate receiver distances between about 200 and 400 km.) Due to the symmetry of our model, the results remain unchanged with respect to sign changes of backazimuth. Near the surface, where the *a*-axis is parallel to the *x*-axis, the fast polarization is close to 0° for the three cases. Initial values at 400 km depth vary between -30° and 80°. For $\phi_b = 160^\circ$ the fast polarization changes most rapidly at a depth of about 150 km. These results correspond to the surface-projected ray paths given in Fig. 1. Accumulated delay times increase continuously along the rays and reach values between 1.3 and 2.8 s. For $\phi_b = 160^\circ$ the ray passes by the centre of the plume most closely (see Fig. 1).

To understand the variation of fast polarizations for this case ($\phi_b = 160^\circ$) in detail, we show fast polarizations that have been calculated from the elastic constants c_{ijkl} (eq. 14) at five different positions along the reference path (Fig. 7). The polarizations are given at angular distances between $\theta = 0^\circ$ and 30° from the vertical, and for the complete azimuthal range (360°). The polarization at the centre of each figure corresponds to the fast polarization of a vertically travelling shear wave (at the given position). Initially, at 400 km depth, the reference ray is close to the central upwelling, where the *a*-axis is nearly vertical. Here, the fast polarization for vertical propagation is oriented at about 45°, which is in correspondence with the (momentary) azimuthal position of the ray (*cf.* Fig. 1). With decreasing depth, the reference ray travels closer to the *x*-axis and the central fast polarization changes continuously to reach a value of 0° at the surface. The fast polarization for a ray at $\phi_b = 160^\circ$ and a vertical incidence angle of 30° changes most rapidly in the depth range between 200 and 100 km, where the anisotropy is weakest. This corresponds to the results given in Fig. 6.

In Fig. 8, we show the corresponding apparent splitting parameters as a function of the initial polarization ϕ_i. For $\phi_b = 40^\circ$, the apparent fast polarization ϕ_a is close to 20° for most values of ϕ_i, and it is approximately equal to the average fast polarization within the medium. The apparent fast axis changes abruptly from $\phi_a = 20^\circ$ to -60° near $\phi_i = 20^\circ$. This is similar for models with continuously varying anisotropy (Rümpker & Silver 1998). The apparent delay times exhibit values between 0.5 and 4 s. For $\phi_b = 100^\circ$, the variations of splitting parameters occur over a larger range between $\phi_i = 45^\circ$ and $\phi_i = 70^\circ$. Within this range the differences between ϕ_a and true fast polarizations in the medium are most significant. For $\phi_b = 160^\circ$ apparent delay times are smaller. The splitting is relatively weak in the range where the apparent splitting parameters vary most. Otherwise, ϕ_a is close to 0°, which is about the average fast polarization in the medium along the reference ray (Fig. 6).

The calculation of apparent splitting parameters breaks down at higher frequencies when more than two parameters

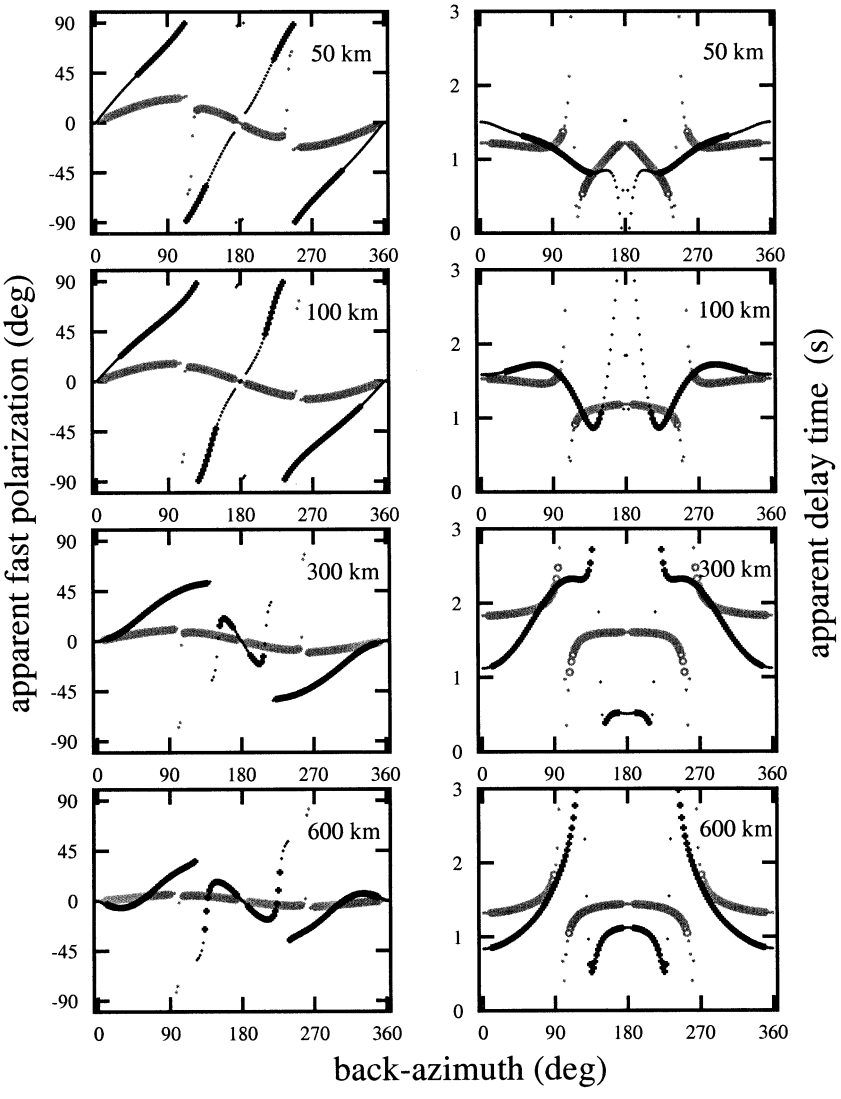

Figure 5. Apparent splitting parameters for *SKS* as functions of backazimuth at four receiver positions along $y=0$ (Fig. 1). The values are given for incident angles of (grey) $\theta=5^\circ$ and (black) $\theta=25^\circ$. The smaller symbols denote relatively weak effects of anisotropy with values of $q<0.15$. The dominant period is 8 s.

are required to characterize the anisotropic effects. To study teleseismic splitting effects at shorter periods ($T=2$ s), we show waveforms corresponding to the ray paths assumed in Fig. 6. The results are given at four initial polarizations, $\phi_i=0^\circ$, 30°, 60° and 90° (Fig. 9). We assume a Gaussian incident waveform to simplify the interpretation of the results. The effects of anisotropy are somewhat more drastic for the first two examples ($\phi_b=40^\circ$ and $\phi_b=100^\circ$), which is in agreement with larger accumulated delay times. In both cases there are distinct fast and slow arrivals that are separated by about 2 and 3 s, respectively. The individual arrivals exhibit both radial and transverse components, which is in contrast to the characteristics of longer-period shear wave splitting. A single dominant (fast or slow) arrival occurs whenever ϕ_i is parallel or perpendicular to the fast polarization at the base. This is the case for $\phi_i=30^\circ$ (at a backazimuth $\phi_b=40^\circ$) and for $\phi_i=0^\circ$, 90° (at a backazimuth $\phi_b=100^\circ$). The accumulated delay time is relatively small for $\phi_b=160^\circ$, which is related to large-amplitude arrivals with little time delay (or advance). The short-period waveforms shown here do not exhibit the 90° periodicity of the long-period apparent splitting parameters. For example, the waveforms at $\phi_i=0^\circ$ and $\phi_i=90^\circ$ are time-reversed. However, this relation is strictly valid only for (unrealistic) Gaussian and similar symmetric waveforms.

4 DISCUSSION AND CONCLUSIONS

We have applied the forward-propagator method to calculate apparent splitting parameters and waveforms for weakly anisotropic 3-D media. The incremental propagators are constructed from local values of the fast polarization and of the qS slowness differences along a reference ray in an isotropic background medium. The complete propagator is then obtained by matrix multiplication. The method allows the calculation of two apparent splitting parameters that can be compared directly with results from splitting observations. In smoothly varying media the forward-propagator seismogram is equivalent to the common ray theory of Coates & Chapman (1990).

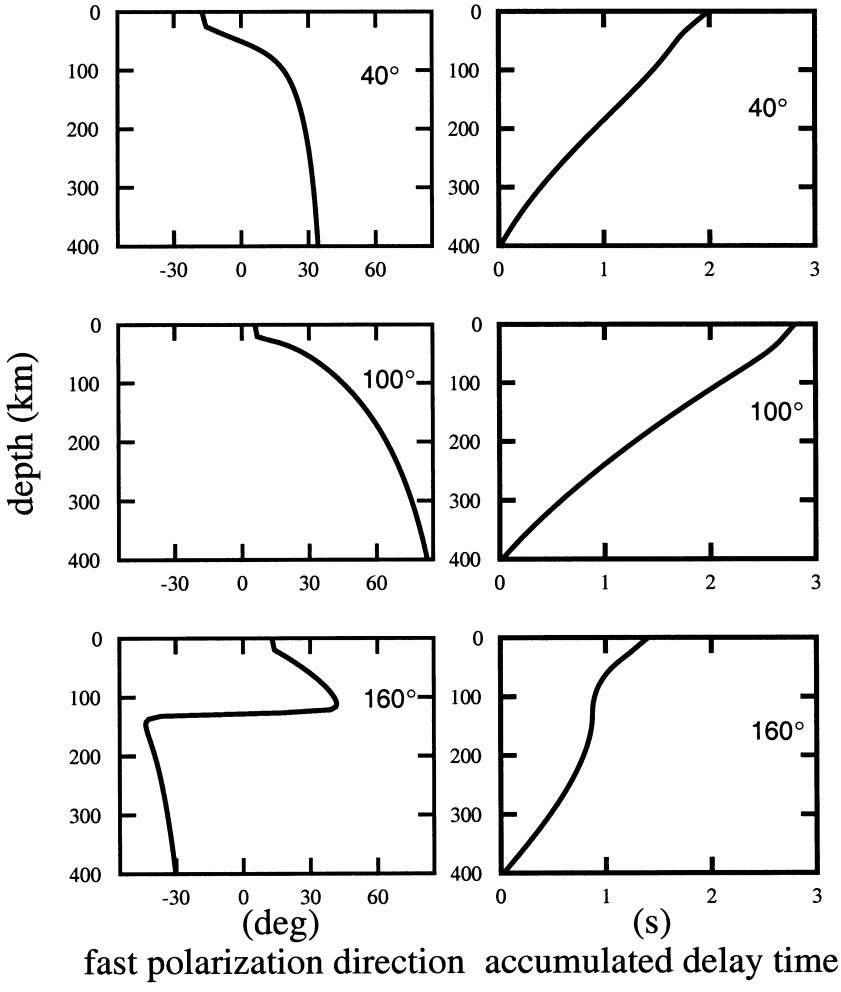

Figure 6. The true fast polarization directions and the accumulated delay times as functions of depth for three reference rays arriving at the receiver with coordinates $x = 300$ km and $y = 0$ km (see Fig. 1). The results are shown for reference rays with backazimuths of 40°, 100° and 160°. The vertical angle of incidence is 30° for the three cases.

The comparison with finite difference calculations shows that the method may be applied to the forward modelling of shear wave splitting in media with complex variations of anisotropy such as mantle plumes and subduction zones. It can be used to combine fluid dynamic and seismic modelling to study the wave effects of upper mantle deformation and flow processes. However, the method is not applicable to strongly anisotropic media, where the two *qS* waves propagate independently along separate ray paths. Thus, it is more appropriate for long-period teleseismic *S* and *SKS* phases. Also, since the calculations are based on rays in an isotropic reference medium, the method is limited in situations where isotropic ray theory can be used. Regions with wave front triplications due to slowness surface indentations are therefore excluded (Rümpker & Thomson 1994). For relatively plane and long-period teleseismic phases, the effect is probably not significant. In principle, this limitation can be overcome by combination with slowness integration methods (e.g. Kendall & Thomson 1993b).

We have applied our method to the calculation splitting parameters for plume-type anisotropic variations in the upper mantle. For an incoming *SKS* wave, the waveforms and splitting parameters exhibit the following characteristics.

(1) Anisotropic effects on waveforms are expected to be weak for rays that arrive at receivers above the central upwelling at radial distances < 100 km. This is due to the combined effects of initial polarization (backazimuth) and vertical *a*-axis orientation. Anisotropic effects are expected to be most pronounced at distances between 150 and 450 km, where the *a*-axis aligns horizontally in the upper part of the model. This corresponds to backazimuths close to $\pm 45°$ and $\pm 135°$ at steep incidence (5°), and to backazimuths close to $\pm 90°$ at shallower incidence (25°) (see Fig. 4).

(2) The average delay times reach a maximum at a distance of about 300 km away from the centre (see Fig. 5). The initial increase is a result of the reorientation of the *a*-axes from the vertical to the horizontal direction. Observations of delay-time increases with distance from an ocean ridge at stations near the East Pacific Rise (Wolfe & Solomon 1998) may possibly result from a similar mechanism.

(3) The variability of the apparent splitting parameters as functions of backazimuth increases for stations that are closer to the central upwelling and for rays at shallower incidence angle (see Fig. 5).

(4) At stations near the central upwelling, the apparent fast polarizations at steep incidence cover an angular range of

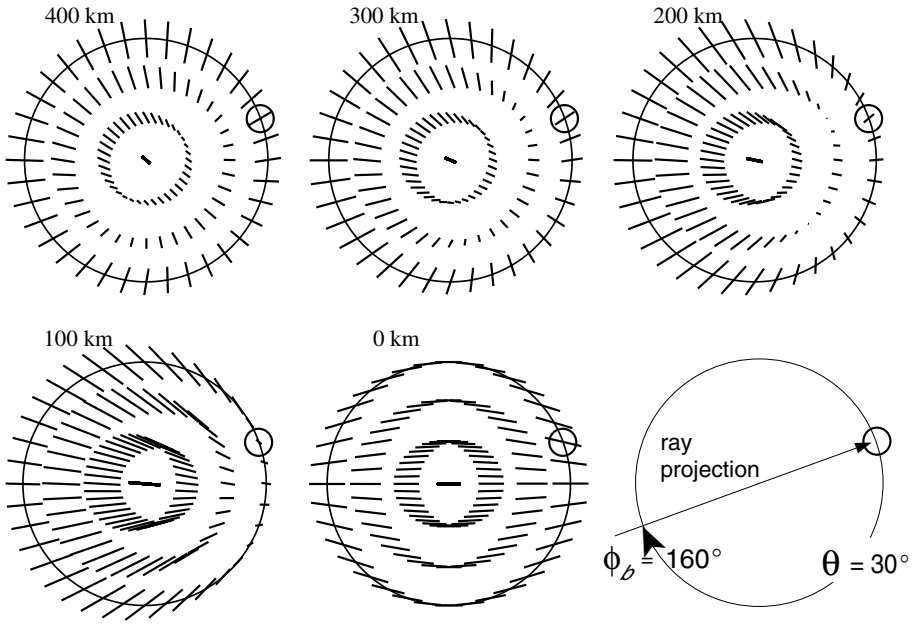

Figure 7. Fast polarizations (solid bars) calculated from the elastic constants at five positions along the reference ray path with a backazimuth of 160° (Figs 1 and 6). Values in kilometres denote depth. The fast polarizations are shown at increments of 10° for both backazimuth and vertical angle of incidence. The large circle corresponds to a vertical incidence angle, θ, of 30°. The small circles indicate the fast polarizations for a ray with a backazimuth of 160° and a vertical incidence angle of $\theta = 30°$, which corresponds to the third example given in Fig. 6. The bars are scaled with respect to the strength of anisotropy.

about 50° as functions of backazimuth. The results at shallower incidence are even more variable but the anisotropic effects are less pronounced for a wide range of back azimuths (see Fig. 5). For a given backazimuth, apparent fast polarizations for the two extreme angles of incidence may differ by up to 70°.

(5) At larger distances (>100 km), splitting parameters slowly converge to values expected for homogeneous media. The observed fast axes are more or less parallel to the horizontal flow directions. The average delay times decrease further with increasing distance.

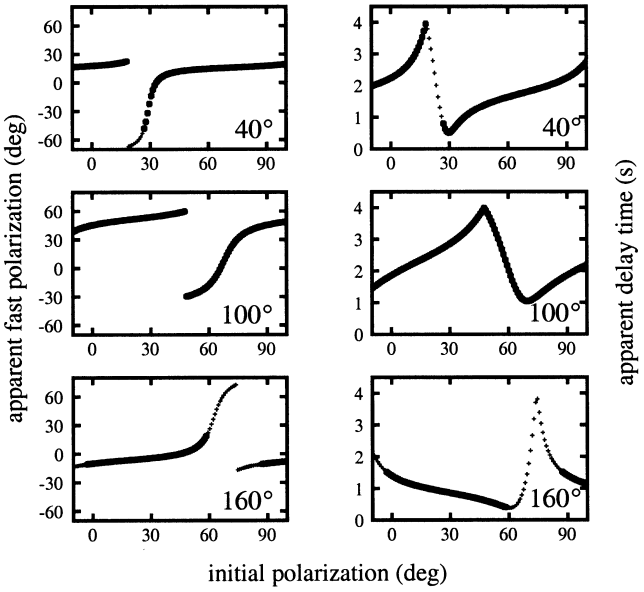

Figure 8. Apparent splitting parameters for S as functions of initial polarization for the three reference rays ($\phi_b = 40°$, 100°, 160°) of Fig. 6. Large symbols correspond to values of $q > 0.15$. The dominant period is 8 s.

For teleseismic S at an incidence angle of $\theta = 30°$, we observe the following.

(1) For a fixed ray path the apparent splitting parameters exhibit the familiar 90° periodicity as functions of initial polarization (not backazimuth!).

(2) Generally, the apparent fast polarizations are close to the average fast polarization in the medium along the reference ray. Larger deviations coincide with rapidly varying apparent delay time as a function of backazimuth.

(3) Shorter-period ($T = 2$ s) waveforms show distinct fast and slow arrivals, each containing radial and transverse displacement components. The corresponding displacement amplitudes are sensitive to the initial polarization.

Note that the distance estimates given here only apply to the specific plume model used in our calculations. However, we think that the model exhibits general characteristics of plume-type upwellings in the upper mantle and that the results provide a guide for future modelling based on mineral texture development. Our results indicate that direct evidence for mantle plumes from shear wave splitting is more likely to come from stations at some distance away from the central upwelling. This suggests the deployment of OBS stations around proposed mantle plumes such as Hawaii or Galapagos to detect their characteristic flow fields in future seismological experiments. The calculation of splitting parameters based on fluid dynamical models of mineral texture development is the next step in our effort to model anisotropic mantle plumes.

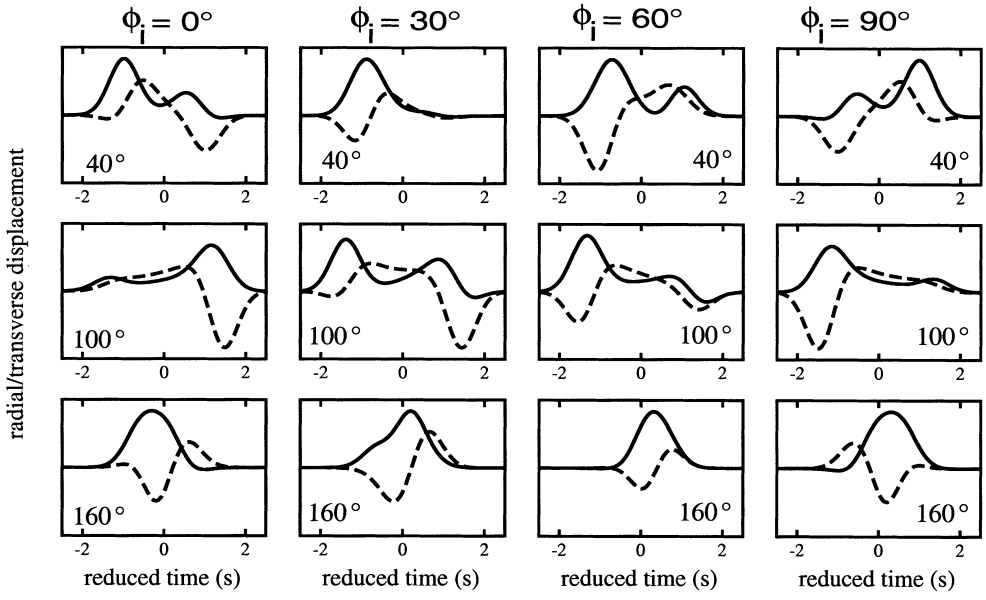

Figure 9. Radial (solid line) and transverse (dashed line) waveforms as functions of initial polarization for the three cases ($\phi_b = 40°$, 100°, 160°) given in Fig. 6. The dominant period is 2 s.

ACKNOWLEDGMENTS

We are grateful to Karen Fischer and Martha Savage for constructive reviews.

REFERENCES

Blackman, D.K. & Kendall, J.-M., 1997. Sensitivity of teleseismic body waves to mineral texture and melt in the mantle beneath a mid-ocean ridge, *Phil. Trans. R. Soc. Lond.,* A**355,** 217–231.

Blackman, D.K., Kendall, J.-M., Dawson, P.R., Wenk, H.-R., Boyce, D. & Phipps-Morgan, J., 1996. Teleseismic imaging of subaxial flow at mid-ocean ridges: traveltime effects of anisotropic mineral texture in the mantle, *Geophys. J. Int.,* **127,** 415–426.

Červený, V., 1987. Ray tracing algorithms in laterally varying layered structures, in *Seismic Tomography, with Applications in Global Seismology and Exploration Geophysics,* pp. 99–133, ed. Nolet, G., D. Reidel, Dordrecht.

Chapman, C.H. & Shearer, P.M., 1989. Ray tracing in azimuthally anisotropic media—II. Quasi-shear wave coupling, *Geophys. J. Int.,* **96,** 65–83.

Chastel, Y.B., Dawson, P.R., Wenk, H.-R. & Bennet, K., 1993. Anisotropic convection with implications for the upper mantle, *J. geophys. Res.,* **98,** 17 757–17 771.

Coates, R.T. & Chapman, C.H., 1990. Quasi-shear wave coupling in weakly anisotropic 3-D media, *Geophys. J. Int.,* **103,** 301–320.

Crampin, S., 1981. A review of wave motion in anisotropic and cracked elastic media, *Wave Motion,* **3,** 343–391.

Dawson, P.R. & Wenk, H.-R., 1997. Is texturing of the upper mantle a cause of seismic heterogeneity?, *EOS, Trans. Am. geophys. Un.,* **78,** 482.

Fouch, M.J., Fischer, K.M., Parmentier, E.M., Wysession, M.E. & Clarke, T.J., 2000. Shear wave splitting, continental keels, and patterns of mantle flow, *J. geophys. Res.,* **105,** 6255–6276.

Hall, C.E., Fischer, K.M., Parmentier, E.M. & Blackman, D., 2000. The influence of plate motions on three dimensional back-arc mantle flow and shear wave splitting, *J. geophys. Res.,* in press.

Jech, J. & Pšenčík, X., 1989. First-order perturbation method for anisotropic media, *Geophys. J. Int.,* **99,** 369–376.

Kendall, J.-M. & Thomson, C.J., 1993. Seismic modelling of subduction zones with inhomogeneity and anisotropy—I. Teleseismic *P*-wave front tracking, *Geophys. J. Int.,* **112,** 39–66.

Kendall, J.-M. & Thomson, C.J., 1993. Maslov ray summation, *Geophys. J. Int.,* **113,** 186–214.

Kennett, B.L.N. & Engdahl, E.R., 1991. Traveltimes for global earthquake location and phase identification, *Geophys. J. Int.,* **105,** 429–465.

Kumazawa, M. & Anderson, O.L., 1969. Elastic moduli, *J. geophys. Res.,* **25,** 5961–5972.

Landau, L.D. & Lifshitz, E.M., 1977. *Quantum Mechanics—Nonrelativistic Theory,* Pergamon Press, Oxford.

Mainprice, D. & Silver, P.G., 1993. Interpretation of *SKS*-waves using samples from the subcontinental lithosphere, *Phys. Earth planet. Inter.,* **78,** 257–280.

Martin, B.E. & Thomson, C.J., 1997. Modelling surface waves in anisotropic structures II: examples, *Phys. Earth planet. Inter.,* **103,** 253–279.

McKenzie, D.P., 1979. Finite deformation during fluid flow, *Geophys. J. R. astr. Soc.,* **58,** 689–715.

Musgrave, M.J.P., 1970. *Crystal Acoustics,* Holden–Day, San Francisco, CA.

Nicolas, A. & Christensen, N.I., 1987. Formation of anisotropy in upper mantle peridotites—a review, in *Composition, Structure and Dynamics of the Lithosphere–Asthenosphere System, AGU Geodyn. Ser.,* Vol. 16, pp. 111–123, eds Fuchs, K. & Froidevaux, C., AGU, Washington, DC.

Peselnik, L. & Nicolas, A., 1978. Seismic anisotropy in an ophiolite peridotite: application to oceanic upper mantle, *J. geophys. Res.,* **83,** 1227–1235.

Pšenčík, I., 1998. Green's function for inhomogeneous weakly anisotropic media, *Geophys. J. Int.,* **135,** 279–288.

Ribe, N.M. & Christensen, U.R., 1994. Three-dimensional modeling of plume-lithosphere interaction, *J. geophys. Res.,* **99,** 669–682.

Ribe, N.M. & Yu, Y., 1991. A theory for plastic deformation and textural evolution of olivine polycrystals, *J. geophys. Res.,* **96,** 8325–8335.

Rümpker, G., 1996. A parabolic approximation for shear waves in 3D anisotropic media, *EOS, Trans. Am. geophys. Un. Fall Mtng Suppl.,* 523.

Rümpker, G. & Silver, P.G., 1998. Apparent shear-wave splitting parameters in the presence of vertically varying anisotropy, *Geophys. J. Int.,* **135,** 790–800.

Rümpker, G. & Thomson, C.J., 1994. Seismic-waveform effects of conical points in gradually varying anisotropic media, *Geophys. J. Int.,* **118,** 759–780.

Rümpker, G., Tommasi, A. & Kendall, J.-M., 1999. Numerical simulations of depth-dependent anisotropy and frequency-dependent wave propagation effects, *J. geophys. Res.*, **104,** 23 141–23 153.

Savage, M.K. & Sheehan, A.F., 2000. Seismic anisotropy and mantle flow from the Great Basin to the Great Plains, *J. geophys. Res.,* in press.

Sharafutdinov, V.A., 1994. Quasi-isotropic approximation in dynamic elasticity and some problems in geotomography, *Russ. Geol. Geophys.,* **35,** 58–71.

Shearer, P.M. & Chapman, C.H., 1989. Ray tracing in azimuthally anisotropic media—I. Results for models of aligned cracks in the upper crust, *Geophys. J. Int.,* **96,** 51–64.

Silver, P.G. & Chan, W.W., 1991. Shear wave splitting and subcontinental mantle deformation, *J. geophys. Res.,* **96,** 16 429–16 454.

Silver, P.G. & Savage, M.K., 1994. The interpretation of shear-wave splitting parameters in the presence of two anisotropic layers, *Geophys. J. Int.,* **119,** 949–963.

Silver, P.G., Mainprice, D., Ismail, W.B., Tommasi, A. & Barruol, G., 1999. Mantle structural geology from seismic anisotropy, in *Mantle Petrology: Field Observations and High Pressure Experimentation: A Tribute to Francis R. (Joe) Boyd,* pp. 79–103, eds Fei, Y., Bertka, C.M. & Mysen, B.O., Spec. Publ. No. 6, Geochemical Society, Houston, Tx.

Tommasi, A., 1998. Forward modeling of the development of seismic anisotropy in the upper mantle, *Earth planet. Sci. Lett.,* **160,** 1–13.

Tommasi, A., Vauchez, A. & Russo, R., 1996. Seismic anisotropy in ocean basins: resistive drag of sublithospheric mantle?, *Geophys. Res. Lett.,* **23,** 2991–2994.

Verma, R.K., 1960. Elasticity of some high-density crystals, *J. geophys. Res.,* **65,** 757–766.

Vinnik, L.P. & Kind, R., 1993. Ellipticity in teleseismic *S*-particle motion, *Geophys. J. Int.,* **113,** 165–174.

Wenk, H.-R., Bennett, K., Canova, G.R. & Molinari, A., 1991. Modeling plastic deformation of peridotite with a self-consistent theory, *J. geophys. Res.,* **96,** 8337–8349.

Wolfe, X., Solomon, X., 1998. Shear-wave splitting and implications for mantle flow beneath the MELT region of the East Pacific Rise, *Science,* **280,** 1230–1232.

Zillmer, M., Kashtan, B.M. & Gajewski, D., 1998. Quasi-isotropic approximation of ray theory for anisotropic media, *Geophys. J. Int.,* **132,** 643–653.

APPENDIX A: COMPARISON WITH COUPLING RAY THEORY

We show the equivalence of the forward propagator and the coupling ray theory of Coates & Chapman (1990). First, the right-hand side of (6) is multiplied by the previously omitted factor, $\exp[i\omega(p_f-p_s)\Delta x/2]$, which accounts for the correct advance of the reference ray in the time domain. In view of (3), this leads to

$$\begin{pmatrix} u_k^{(f)} \\ u_k^{(s)} \end{pmatrix} = \begin{pmatrix} \cos\Delta\xi\ \mathrm{e}^{+i\omega p_f\Delta x} & \sin\Delta\xi\ \mathrm{e}^{+i\omega p_f\Delta x} \\ -\sin\Delta\xi\ \mathrm{e}^{+i\omega p_s\Delta x} & \cos\Delta\xi\ \mathrm{e}^{+i\omega p_s\Delta x} \end{pmatrix} \begin{pmatrix} u_{k-1}^{(f)} \\ u_{k-1}^{(s)} \end{pmatrix}. \tag{A1}$$

Furthermore, we take a ray ansatz of the form

$$u_{k-1}^{(f)} = U_{k-1}^{(f)}\ \mathrm{e}^{+i\omega\int_0^x p_f(\zeta)d\zeta}, \qquad u_k^{(f)} = U_k^{(f)}\ \mathrm{e}^{+i\omega\int_0^{x+\Delta x} p_f(\zeta)d\zeta} \tag{A2}$$

(similarly for $u_{k-1}^{(s)}$, $u_k^{(s)}$), where $U_{k-1}^{(f)}$ and $U_k^{(f)}$ denote the ray amplitudes before and after the ray has passed the incremental distance Δx, respectively. The corresponding time advance is accounted for by the phase factor. After multiplying the first equation (A1) by $\exp[-i\omega\int_0^x p_f(\zeta)\,d\zeta]$ and the second by $\exp[-i\omega\int_0^x p_s(\zeta)\,d\zeta]$, we obtain a system for the ray amplitudes:

$$\begin{pmatrix} U_k^{(f)} \\ U_k^{(s)} \end{pmatrix} = \begin{pmatrix} \cos\Delta\xi & \sin\Delta\xi\ \mathrm{e}^{+i\omega\int_0^x (p_s-p_f)d\zeta} \\ -\sin\Delta\xi\ \mathrm{e}^{-i\omega\int_0^x (p_s-p_f)d\zeta} & \cos\Delta\xi \end{pmatrix} \times \begin{pmatrix} U_{k-1}^{(f)} \\ U_{k-1}^{(s)} \end{pmatrix}, \tag{A3}$$

where we have used the fact that $p_f\Delta x$ may be expressed as $\int_x^{x+\Delta x} p_f(\zeta)d\zeta$ (similarly for $p_s\Delta x$). Taking limiting expressions such as

$$\lim_{\Delta x\to 0} \frac{(U_k^{(f)} - U_{k-1}^{(f)})}{\Delta x} = \frac{dU^{(f)}}{dx} \tag{A4}$$

yields a differential system for the ray amplitudes,

$$\frac{d}{dx}\begin{pmatrix} U^{(f)} \\ U^{(s)} \end{pmatrix} = \begin{pmatrix} 0 & \frac{d\xi}{dx}\ \mathrm{e}^{+i\omega\int_0^x (p_s-p_f)d\zeta} \\ -\frac{d\xi}{dx}\ \mathrm{e}^{-i\omega\int_0^x (p_s-p_f)d\zeta} & 0 \end{pmatrix} \times \begin{pmatrix} U^{(f)} \\ U^{(s)} \end{pmatrix}, \tag{A5}$$

where we have used the fact that $\cos\Delta\xi\to 1$ and $\sin\Delta\xi\to\Delta\xi$ in the limit $\Delta x\to 0$. We thus assume the continuous variation of polarization ξ along the reference ray. The system (A5) formally agrees with the coupling equations of Coates & Chapman (1990, eq. 31). The coupling coefficient $d\xi/dx$ relates directly to the rotation of polarization along the ray path; the exponential accounts for the accumulated separation between fast and slow shear waves. A slightly modified version of (A5) was used by Chapman & Shearer (1989) to study coupling effects due to slowness surface singularities (e.g. Crampin 1981) in laterally homogeneous media. The combination with 2-D Maslov slowness integrals allows coupling calculations for complex wave front features such as cups and swallowtails (Rümpker & Thomson 1994). We have shown that the two formulations (6) and (A5) are equivalent under the condition that the polarization ξ is smoothly varying along the reference ray. Strictly speaking, (A5) is not valid whenever polarization changes discontinuously, for example, at slowness surface singularities. However, meaningful numerical results may still be obtained (see Coates & Chapman 1990). Such problems can be avoided by use of the forward-propagator method for the calculation of the displacement. The propagator is given in terms of incremental delay times and polarization, which can be calculated easily for a given reference ray in the anisotropic region.

APPENDIX B: APPARENT SPLITTING PARAMETERS

Apparent splitting parameters can be calculated under the assumption that anisotropic effects on the incident waveform are caused by a single anisotropic layer. In this case, the splitting may be characterized by the apparent polarization of the fast shear wave (ξ_a) and by the apparent delay time between

fast and slow shear waves (δt_a). The expressions for apparent splitting parameters in multilayered media (Rümpker & Silver 1998) can be applied directly to our present formulation for 3-D weakly anisotropic media.

Writing the initial displacement of a ray incident from an isotropic region in the form $\mathbf{u}_0 = u_0(\hat{\mathbf{p}}, 0)^T$, eq. (13) can be given in the form

$$\begin{pmatrix} a & b \\ -\bar{b} & \bar{a} \end{pmatrix} \begin{pmatrix} \hat{\mathbf{p}} \\ 0 \end{pmatrix} = K \begin{pmatrix} a_a & b_a \\ -\bar{b}_a & \bar{a}_a \end{pmatrix} \begin{pmatrix} \hat{\mathbf{p}} \\ 0 \end{pmatrix}, \tag{B1}$$

where a, b are the elements of the complete forward propagator $\mathbf{\Gamma}_{N,1}^{(p)}$ and a_a, b_a are elements of the apparent splitting operator $\mathbf{\Gamma}_a$. Using (12), the latter are given by

$$a_a = \cos\theta_a - i \sin\theta_a \cos\alpha_a\,, \qquad b_a = -i \sin\theta_a \sin\alpha_a\,. \tag{B2}$$

The elimination of K and separation into real and imaginary parts yields

$$\tan\theta_a = \frac{-b^R}{a^I \sin\alpha_a - b^I \cos\alpha_a} = \frac{-b^I}{b^R \cos\alpha_a + a^R \sin\alpha_a} \tag{B3}$$

(superscripts denote real and imaginary parts), which, after elimination of $\tan\theta_a$, yields

$$\tan\alpha_a = \frac{(b^R)^2 + (b^I)^2}{a^I b^I - a^R b^R}\,, \tag{B4}$$

where

$$\theta_a = \omega \delta t_a / 2\,, \qquad \alpha_a = 2(\phi_a - \phi_0) \tag{B5}$$

and ϕ_0 denotes the polarization direction of the incident shear wave with respect to a global coordinate system.